Fabrication and characterization of high contrast mid-infrared $GeTe_4$ channel waveguides

Vinita Mittal*, Armen Aghajani, Lewis G. Carpenter, James C. Gates, Jonathan Butement, Peter G. R. Smith, James S. Wilkinson and Ganapathy Senthil Murugan

Optoelectronics Research Centre, University of Southampton, Southampton, SO17 1BJ United Kingdom
*

Corresponding author: V.Mittal@soton.ac.uk

We report the fabrication and characterization of high index contrast ($\Delta n \approx 0.9$) $GeTe_4$ channel waveguides on ZnSe substrate for evanescent-field based biosensing applications in the mid-infrared spectral region. $GeTe_4$ films were deposited by RF sputtering and characterized for their structure, composition, transparency and dispersion. The lift-off technique was used to pattern the waveguide channels. Waveguiding between 2.5-3.7 µm and 6.4-7.5 µm was demonstrated and mode intensity profile and estimated propagation losses are given for the 3.5 µm wavelength.

The mid-infrared (MIR) spectral region offers great promise for biosensing, as the fundamental vibrations of most organic molecules occur in this region. Waveguide evanescent field based spectroscopy can detect analytes at very low concentrations using their absorption fingerprints, potentially offering high sensitivity and selectivity over a wide range of compounds without labelling [1]. This would enable rapid real time measurement of complex mixtures to identify and quantify species in clinical samples for point of care diagnosis. Recently, GaAs/GaAlAs waveguides operating at a wavelength of 10.3 µm demonstrated a limit of detection of acetic anhydride of 0.05 pL [2,3]. Conventional materials that are well characterized for telecommunications wavelengths are not suitable for the mid-infrared spectral region because of their strong absorption in this region. Chalcogenide materials containing S, Se and Te are well known for their optical transparency and high refractive index [4], which makes them most suitable for mid-infrared sensing applications. Several chalcogenide material compositions are being actively pursued to fabricate waveguides for mid-infrared applications [5-7]. A single mode arsenic-based chalcogenide channel waveguide was demonstrated at λ=8.4 µm and propagation losses were measured. The waveguides were fabricated by direct-writing with a focused HeNe laser beam to define the waveguides, causing photodarkening at visible wavelengths and yielding an increase ($\Delta n \approx 0.04$) in the refractive index in the MIR [8]. The spectroscopy of a fluoropolymer in the 1500 to 4000 cm^{-1} band has been demonstrated using a waveguide of chalcogenide composition [9]. Recently, the absorption of N-methylaniline at 1496nm was demonstrated using a monolithically integrated chalcogenide waveguide with a microfluidic device and, further, chalcogenide waveguide photonic crystal (PhC) cavity devices were fabricated for spectroscopic chemical sensing [10,11]. $GeTe_4$ rib waveguides fabricated on $Te_{75}Ge_{15}Ga_{10}$ bulk glass substrates were explored in the mid-infrared range of 6-20 µm for spatial interferometry in the search for earth-like planets, where the refractive index contrast between the core and the substrate was about $\Delta n \approx 0.04$ and the film thickness was ~24 µm to allow single mode operation at wavelengths between 10 µm and 20 µm [12-14].

The present work is focused on realizing waveguides for evanescent field based sensing in the mid-infrared wavelength region. A "high refractive index contrast" configuration with a $GeTe_4$ core layer and ZnSe as the substrate, with refractive indices of 3.34 and 2.43 respectively, at a wavelength of 3.5 µm has been chosen. High index contrast between the core and the substrate ($\Delta n \approx 0.9$) allows the highest evanescent power and highest surface sensitivity at the waveguide/analyte interface for evanescent spectroscopy [1]. Earlier, we reported fabrication of rib waveguides with the same combination of core and substrate material, but using reactive ion etching to define the waveguide channels [15] and preliminary results on waveguiding in only the mid wave band (2.5 – 3.7 µm) [16]. In this paper, we describe the deposition of $GeTe_4$ films with structural, morphological, compositional and optical characterization, fabrication of $GeTe_4$ channel waveguide on ZnSe substrate using the lift off technique, end facet preparation by ductile dicing and finally we demonstrate waveguiding in the 2.5–3.7 µm and 6.4 – 7.5 µm spectral regions in addition to the measured mode profile and propagation losses in the 2.5 – 3.7 µm band. The channels are expected to be highly multimoded for these wavelength ranges. A multimode waveguide design was selected in order to establish waveguiding at longer wavelengths (up to 12 µm) with sufficient coupling efficiency using commercially available single mode fibers having core diameters of about 30µm.

$GeTe_4$ films were deposited on 2 mm thick and 50 mm x 50 mm square polycrystalline ZnSe substrates by RF magnetron sputtering in an argon atmosphere. Several films were deposited at different temperatures to study the effect of deposition temperature on film properties. However, the waveguides presented in this paper were fabricated using films deposited at room temperature. Deposition parameters such as sputtering power, pressure, and argon flow rate were varied to optimize the deposition rate. The thickness of the films was

measured using a KLA Tencor stylus profilometer. Amorphous films are desired to prevent excess scattering of propagating modes at grain boundaries. The amorphous nature of the deposited films was determined by using a Rigaku X-ray Diffraction system with monochromatic Cu kα radiation in the 2 theta geometry at a grazing angle of 1°. A Zeiss Scanning electron microscope (SEM) and a Veeco atomic force microscope (AFM) (in tapping mode) were used to observe the film surface morphology and roughness, respectively. X-ray photoelectron spectroscopy (XPS, Thermo Scientific) was used to determine the composition of the film. XPS depth profiles of the $GeTe_4$ films were acquired by etching the film surface with an argon ion beam for fixed time intervals and recording XPS spectra at each depth. To relate the etch depth to the time interval, etching was performed on a film of known thickness until the substrate was visible. The etch rate of the $GeTe_4$ films was found to be ~ 40 nm/minute. The refractive index (n) and extinction coefficient (k) for the ZnSe substrate and the $GeTe_4$ film were measured using ellipsometry (IR-VASE Woollam Co. Inc.) for the wavelength range of 2 µm – 30 µm.

The lift-off technique was used to fabricate the channel waveguides. An 8µm thick layer of lift-off resist LOR 30B (Micro Chem) was spun on a cleaned ZnSe substrate in two steps, followed by a 1.3 µm thick film of S1813 (Shipley) photoresist. The sample was then UV-exposed through a photomask comprising straight channels of varying widths and developed to create the desired undercut profile [17]. A $GeTe_4$ film of about 4.6 µm thickness was deposited onto the patterned resist by RF sputtering as discussed above. Finally, the resist was lifted off in resist stripper SVC-14 (Dow) to obtain the desired waveguide channels. The width of the channels ranged from 15 – 35 µm and they were separated by 100 µm, center to center. An optimized ductile dicing procedure was used to machine the $GeTe_4$ waveguide end facets. The ductile dicing process creating smooth, chip free, low loss waveguide facets; more details on the ductile dicing procedure can be found in Refs [16] & [18]. Surface roughness was obtained with a white light interferometer (Zemetrics, ZeScope). An OPO based tunable source (M-Squared Lasers) and an InSb mid-infrared camera (FLIR) were used for waveguide characterization in the 2.5–3.7 µm spectral region. Light from the OPO was focused with a 0.25 NA ZnSe objective lens into a single mode ZrF_4 fiber with a core of 9 µm diameter (Thorlabs). The other end of the fiber was butt-coupled into the input facet of the channel waveguide and the output was imaged on the mid-infrared camera from the top and at the output cross-section. For waveguide characterization at 6.4–7.5 µm, light from a tunable QCL (Pranalytica) was coupled into the waveguide end facet using a single mode As_2Se_3 fiber with a core diameter of about 30 µm (Coractive). The output was imaged using a microbolometer based mid-infrared camera (Xenics-Gobi 640) from the top. A schematic of the experimental set up is shown in Fig. 1.

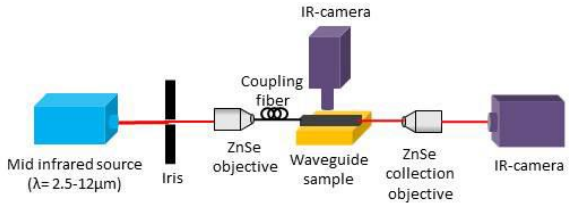

Fig. 1 Experimental apparatus for optical characterization of the waveguides

The $GeTe_4$ deposition rate was measured as a function of sputtering pressure and sputtering power at room temperature. The sputtering pressure was varied from 3mTorr to 30mTorr at a fixed power of 50 W and an Ar flow rate of 20 sccm. The sputtering power was varied from 30 W to 60 W at a fixed sputtering pressure of 10 mTorr and a fixed Ar flow rate of 25 sccm. It was found that the deposition rate decreases with sputtering pressure and increases with sputtering power as expected. A sputtering pressure of 10 – 15 mTorr and power of 40–50 W yielded visibly defect free films with a deposition rate of 0.6-0.7µm/h [15]. Fig. 2(a) shows a cross-section of a 2 µm thick $GeTe_4$ film deposited on a ZnSe substrate at a sputtering pressure of 10 mTorr and sputtering power of 50 W. The film appears dense and free from any columnar structures [19,20]. Since the substrate is polycrystalline, its different planes are visible in the SEM image. Fig. 2(b) shows an SEM image of the $GeTe_4$ channels fabricated by lift-off. Fig. 2(c) depicts the XRD pattern and AFM surface images of ZnSe substrate and $GeTe_4$ film deposited at different temperatures. Fig. 2(c)(i) shows the XRD pattern for the ZnSe substrate and the sharp peaks for the different planes representing its polycrystalline nature. The average (R_a) roughness value for ZnSe substrate is about 2.4 nm. Similarly, Fig. 2 (c)(ii) and (iii) depict the XRD patterns for $GeTe_4$ films deposited at 20°C and 250°C, respectively. The broad curve with no sharp peaks confirms that the deposited films are amorphous. The films remain amorphous over the range of sputtering powers (30 W to 60 W) and deposition temperatures (20°C to 250°C). The R_a value for the $GeTe_4$ film deposited at 20°C is about 4 nm. Although this value of roughness is insignificant for our application in the mid-infrared wavelengths, we found that this roughness value can be further reduced to below 2 nm when the films are deposited at higher temperatures. The XPS depth analysis of the $GeTe_4$ film showed that a 40 nm surface layer of the film was mostly oxide (about 72%) consisting of GeO and TeO_2. Below a depth of 40 nm it was found that TeO_2 was absent but about 2% of GeO was present throughout the thickness of the film. The ellipsometry data for the $GeTe_4$ film showed a strong absorption peak in the 11 – 16 µm region. Literature confirms that this absorption corresponds to a GeO stretching vibration [21-23], supporting the finding of oxygen contamination in the film as shown by XPS depth profile analysis. This absorption/ contamination is primarily due to the presence of oxides in the starting material, which can be minimized by using purer materials and by protecting the surface of the films by depositing a suitable capping layer. However, the material losses were estimated to be less than 0.1 dB/cm for wavelengths below 10 µm as deduced from extinction coefficient data from the ellipsometry. Further details on the XPS analysis, ellipsometry and FTIR measurements can be found in Ref [15].

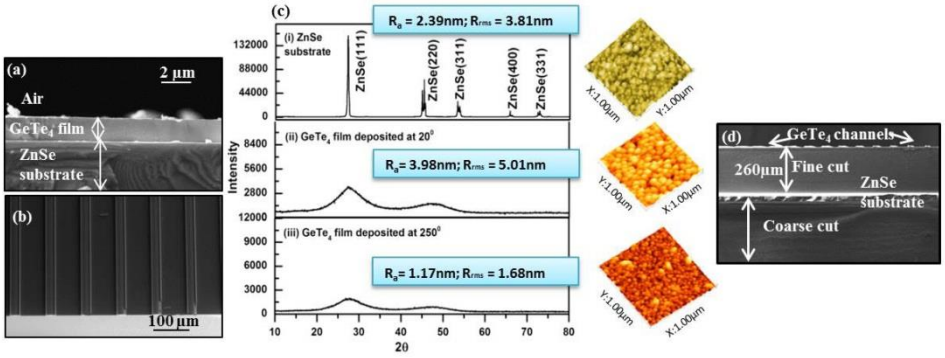

Fig. 2 SEM images of (a) the cleaved cross-section of an as-deposited $GeTe_4$ film, (b) top view of $GeTe_4$ channels fabricated by lift-off, (c) XRD pattern and AFM image of a 1x1 µm2 scan area of (i) a ZnSe substrate and (ii), (iii) a $GeTe_4$ film deposited at a temperature 20°C and 250°C, respectively, and (d) an SEM image of the end facet of the waveguide cut by ductile dicing.

Since ZnSe is a polycrystalline material and $GeTe_4$ is soft compared to commonly used waveguide materials such as silica, silicon and tantala, conventional polishing caused chipping of the edges of the samples when end-facet polishing was attempted. To avoid this problem, precision ductile dicing was employed to saw the end facets. The average surface roughness of the end facets were ~3.0 nm as measured by white light interferometry. An SEM image of the waveguide facet machined in the ductile dicing regime revealing the smooth, chip and pit free surface is shown in Figure 2 (d).

Fig. 3 (a) shows a top view of the output end of the waveguide sample showing light scattered from the end of a 26 µm wide channel at a wavelength of 3.5 µm. The image was captured with the InSb camera and lens, having a resolution of 5 µm, using the configuration shown in Fig 1. The channels are clearly seen in the image. Fig. 3 (b) shows a near-field image of the mode emerging from the same waveguide end-facet captured by replacing the built-in camera lens by an external ZnSe objective lens to further magnify the image by a factor of about 8. Here the infrared image is background corrected, being the difference between the images with the OPO on and off, and is a true thermal image of the temperature difference. The scale of the modal images was calibrated using the known distance between two waveguides. Light guidance was observed over the wavelength range from 2.5 µm to 3.7 µm. On moving the input fiber exactly 100 µm, which is the distance between two waveguides, another channel output is illuminated confirming the confinement of light (as shown in the Media 1 without background correction).

The experimental horizontal and vertical mode profiles were extracted from Fig. 3 (b) and are shown in Fig 3 (c) together with theoretical mode profiles for the fundamental mode calculated using COMSOL. The experimentally measured FWHM mode intensity spot-sizes for the waveguide output intensity distribution in the horizontal and vertical directions of the 26 µm wide channel waveguide are 10.2 µm and 7.8 µm, respectively. The "vertical" direction is defined as normal to the substrate surface. The FWHM spotsizes calculated by COMSOL for the fundamental mode in the horizontal and vertical directions at λ=3.5 µm are 13.2 µm and 2.4 µm respectively. As the waveguide is highly multimoded at this wavelength and the image resolution is ~5 µm, it is unclear which modes have been excited in practice. If the fundamental mode has been excited in the vertical direction, then the measured mode profile compares well with the theoretical mode profile, taking into account the resolution of the imaging system. It is unclear why the measured spotsize in the horizontal direction is smaller than that predicted theoretically. We postulate that the 9 µm core input fiber excites several modes (laterally) in the waveguide and that these self-image along the waveguide, acting like an MMI [24], to produce a narrow resultant intensity distribution at the waveguide output facet.

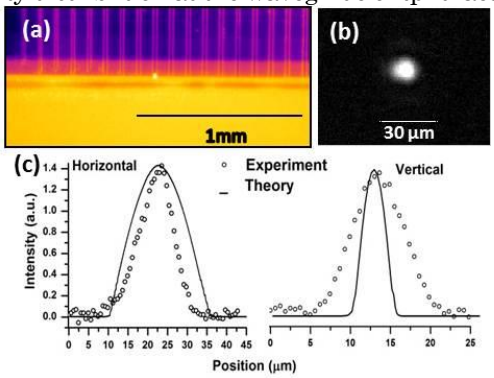

Fig. 3 Infrared images of (a) top view and (b) cross-sectional view of the output facet of a channel waveguide showing light guidance at a wavelength of 3.5 µm (Media 1), (c) measured horizontal and vertical mode profiles with theoretical comparison.

In order to explore waveguide losses, the streak of scattered light at λ=3.5 µm was observed from above the waveguide as shown in Fig. 4. It is clear that there are many large scattering centers along the waveguide in addition to a more uniform scattering distribution. The former are due to imperfections in the lift-off process which has left irregularities on the walls of the channels. The propagation loss calculated from these data was found to be in the range of 1-5 dB/cm, depending upon the region of the image selected for analysis. Work is underway to optimize the liftoff process so as to minimize the scattering defects.

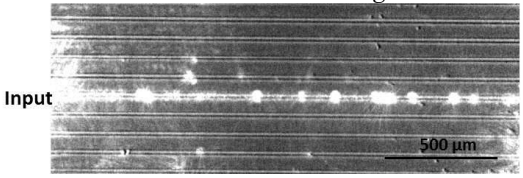

Fig. 4 Infrared image showing streak of light scattered from waveguide

The same waveguide sample was tested at longer wavelengths (6.4−7.5 μm), using the QCL, and found to be guiding light over this full range. Fig. 4 shows infrared images captured at λ=6.8 μm using the mid-infrared camera with its as-supplied lens. Fig. 5 (a) shows the top view of the sample where the channels are clearly visible. Light can be seen emerging from one waveguide end and this region is shown expanded in the inset. On moving the sample exactly 100 μm, the distance between two waveguides, consecutive channels are excited (shown in the Media 2). Fig. 5 (b) shows a cross-sectional image of the sample with a bright spot corresponding to a near-field image of the light emerging from the waveguide end; this is also shown expanded in an inset. On moving the input fiber exactly 100 μm, another channel is excited, confirming guidance at this wavelength (shown in the Media 3).

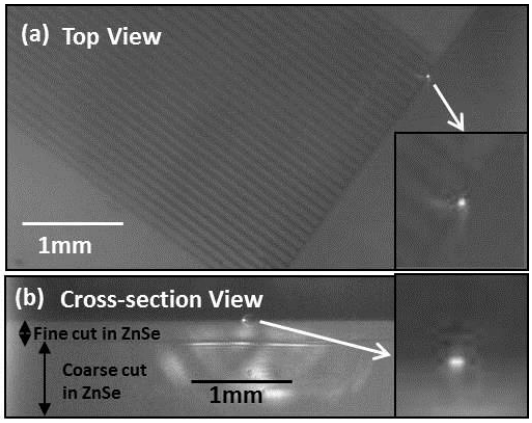

Fig. 5 (a) Top view (Media 2) and (b) cross-section of the infra-red camera image of the output facet of the guiding channel waveguide at 6.8 μm wavelength (Media 3) (insets: magnified image of the guiding channel).

In conclusion, high-contrast germanium telluride channel waveguides have been fabricated on zinc selenide substrates using RF-sputtering and lift-off. The deposited films were found to be amorphous with an average surface roughness below 4 nm and were found to transmit over the spectral range from 2 – 20 μm. Waveguiding was demonstrated in the 2.5−3.7 μm and 6.4 – 7.5 μm wavelength ranges. The mode intensity profile was extracted at a wavelength of 3.5 μm and preliminary estimates of propagation losses were reported. Further improvements in the starting materials and fabrication processes will be used in future to achieve single mode waveguides at longer wavelengths and to perform mid-infrared biosensing experiments with high sensitivity due to the large core-cladding index contrast in these waveguides.

The authors thank the European Research Council under the European Union's Seventh Framework Programme (FP7/2007-2013) ERC grant agreement no. 291216 "Wideband Integrated Photonics for Accessible Biomedical Diagnostics" for funding this work. The authors would also like to acknowledge Neil Sessions, Mike Perry and Owain Clark for the support they have provided in the cleanroom.

References

1. J.S. Wilkinson, *Handbook of Spectroscopy* (Wiley-VCH, Germany, 2014) Günter Gauglitz and David S. Moore (Eds), Ch. 48.
2. X. Wang, M. Sieger and B. Mizaikoff, Proc. SPIE **8631**, 86312M (2013).
3. X. Wang, S-S. Kim, R. Roßbach, M. Jetter, P. Michlerb and B. Mizaikoff, Analyst **137**, 2269 (2012).
4. D. Hewak, Nat. Photon **5**, 474 (2011).
5. C. Vigreux-Bercovici, E. Bonhomme, A. Pradel and J.-E. Broquin, Appl. Phys. Lett. **90**, 011110 (2007).
6. E. Barthélémy, C. Vigreux, G. Parent, M. Barillot, and A. Pradel, Phys. Status Solidi C **8**, 2890 (2011).
7. C.C. Huang, D. Hewak and J. Badding, Opt. Express **12**, 2501 (2004).
8. N. Hô, M. C. Phillips, H. Qiao, P. J. Allen, K. Krishnaswami, B. J. Riley, T. L. Myers and N. C. Anheier, Opt. Lett. **31**, 1860 (2006).
9. P. Ma, D.-Y. Choi, Y. Yu, X. Gai, Z. Yang, S. Debbarma, S. Madden and B. Luther-Davies, Opt. Express 21, 29927 (2013).
10. J. Hu, V. Tarasov, A. Agarwal, L. Kimerling, N. Carlie, L. Petit and K. Richardson, Opt. Express 15, 2307 (2007).
11. V. Singh, P. T. Lin, N. Patel, H. Lin, L. Li, Y. Zou, F. Deng, C. Ni, J. Hu, J. Giammarco, A. P. Soliani, B. Zdyrko, I. Luzinov, S. Novak, J. Novak, P. Wachtel, S. Danto, J. D. Musgraves, K. Richardson, L. C. Kimerling and A. M. Agarwal, Sci. Technol. Adv. Mat. 15, 014603 (2014).
12. C. Vigreux, E. Barthelemy, L. Bastard, J-E. Broquin, M. Barillot, S. Menard, G. Parent and A. Pradel, Opt. Lett. 36, 2922 (2011).
13. C. Vigreux, A. Pradel, L. Bastard, J-E. Broquin, G. Parent, X Zhang and M. Barillot: 13th International Conference on Transparent Optical Networks (ICTON), We.A6.3 (2011).
14. C. Vigreux, M. Barillot, E. Barthelemy, L. Bastard, J-E. Broquin, V. Kirschner, S. Menard, G. Parent, C. Poinsot, A. Pradel, S. Zhang and X. Zhang, Advances in Optical Materials, OSA Technical Digest (CD) (Optical Society of America), AIFB7(2011).
15. V. Mittal, J.S. Wilkinson and G.S. Murugan, Proc. SPIE 8988, 89881A-1 (2014).
16. V. Mittal, L. G. Carpenter, J. C. Gates, J. S. Wilkinson and G. S. Murugan, 12th International Conference on Fiber Optics and Photonics, OSA Technical Digest (online) (Optical Society of America), T4B.4 (2014).
17. J. Golden, H. Miller, D. Nawrocki and J. Ross, CS Mantech Conference, CS Mantech Technical Digest, Tampa, Florida, USA (2009)
18. L. G. Carpenter, H. L. Rogers, P. A. Cooper, C. Holmes, J. C. Gates and P. G. R. Smith, J. Phys. D Appl. Phys. 46, 475103 (2013).
19. C. Vigreux-Bercovici, L. Labadie, J. E. Broquin, P. Kern and A. Pradel, J. Optoelectron. Adv. M. 7, 2625 (2005).
20. V. Balan, C. Vigreux and A. Pradel, J. Optoelectron. Adv. M. 6, 875 (2004).
21. C. Vigreux, E. Bonhomme and A. Pradel, J. Non-Cryst. Solids 353, 1388 (2007).
22. X. H. Zhang, L. Calvez, V. Seznec, H. L. Ma, S. Danto, P. Houizot, C. Boussard-Pledel and J. Lucas, J. Non-Cryst. Solids 352, 2411 (2006).
23. J. Nishii, T. Yamashita and T. Yamagishi, J. Mater. Sci. 24, 4293 (1989).
24. J. S. Yu, J. Y. Moon, S. M. Choi, and Y. T. Lee, Jpn. J. Appl. Phys. 40, 634 (2001).

REFERENCES

1. J.S. Wilkinson, *Handbook of Spectroscopy* (Wiley-VCH, Germany, 2014) Günter Gauglitz and David S. Moore (Eds), Ch. 48.
2. X. Wang, M. Sieger, and B. Mizaikoff, "Toward on-chip mid-infrared chem/bio sensors using quantum cascade lasers and substrate-integrated semiconductor waveguides", Vol. 8631, 86312M, 2013.
3. X. Wang, S-S. Kim, R. Roßbach, M. Jetter, P. Michlerb and B. Mizaikoff, "Ultra-sensitive mid-infrared evanescent field sensors combining thin-film strip waveguides with quantum cascade lasers", Analyst, Vol. 137, no. 10, p. 2269–2522, 2012.
4. D. Hewak, "The promise of chalcogenides," Interview, Nat Photon, Vol. 5, No. 8, p. 474, 2011.
5. C. Vigreux-Bercovici, E. Bonhomme, A. Pradel, J.-E. Broquin, "Transmission measurement at 10.6µm of $Te_2As_3Se_5$ rib waveguides on As_2S_3 substrate", Appl. Phys. Lett., Vol. 90, p. 011110, 2007.
6. E. Barthélémy, C. Vigreux, G. Parent, M. Barillot, and A. Pradel, "Telluride films and waveguides for IR integrated optics", Phys. Status Solidi, Vol. 8, no. 9, p. 2890, 2011.
7. C.C. Huang, D. Hewak, J. Badding, "Deposition and characterization of germanium sulphide glass planar waveguides", Optics Express, Vol. 12, No. 11, p. 2501, 2004.
8. N. Hô, M. C. Phillips, H. Qiao, P. J. Allen, K. Krishnaswami, B. J. Riley, T. L. Myers, and N. C. Anheier, "Single-mode low-loss chalcogenide glass waveguides for the mid-infrared", Opt. Lett., Vol. 31, No. 12, p. 1860, 2006.
9. P. Ma, D.-Y. Choi, Y. Yu, X. Gai, Z. Yang, S. Debbarma, S. Madden, and B. Luther-Davies, "Low-loss chalcogenide waveguides for chemical sensing in the mid-infrared", Opt. Express, Vol. 21, no. 24, p. 29927, 2013.
10. J. Hu, V. Tarasov, A. Agarwal, L. Kimerling, N. Carlie, L. Petit, and K. Richardson, "Fabrication and testing of planar chalcogenide waveguide integrated microfluidic sensor" , Opt. Express, Vol. 15, p. 2307, 2007.
11. V. Singh, P. T. Lin, N. Patel, H. Lin, L. Li, Y. Zou, F. Deng, C. Ni, J. Hu, J. Giammarco, A. P. Soliani, B. Zdyrko, I. Luzinov, S. Novak, J. Novak, P. Wachtel, S. Danto, J. D. Musgraves, K. Richardson, L. C. Kimerling, and A. M. Agarwal, "Mid-infrared materials and devices on a Si platform for optical sensing", Sci. Technol. Adv. Mater., Vol. 15, p. 014603, 2014.
12. C. Vigreux, E. Barthelemy, L. Bastard, J-E. Broquin, M. Barillot, S. Menard, G. Parent and A. Pradel: "Realization of single-mode telluride rib waveguides for mid-infrared applications between 10 and 20µm", Optics Letters, Vol. 36(15), p.2922, 2011
13. C. Vigreux, A. Pradel, L. Bastard, J-E. Broquin, G. Parent, X Zhang and M. Barillot: "All-Telluride Waveguides for Nulling Interferometry in 6-20µm Spectral Range", fabrication and Testing', ICTON 2011.
14. C. Vigreux, M. Barillot, E. Barthelemy, L. Bastard, J-E. Broquin, V. Kirschner, S. Menard, G. Parent, C Poinsot, A. Pradel, S. Zhang, and X. Zhang, "All-telluride channel waveguides for mid-infrared applications", OSA/AIOM 2011.
15. V. Mittal, J.S. Wilkinson, G.S. Murugan, "High contrast GeTe4 waveguides for mid-infrared biomedical sensing applications", Proc. of SPIE, Vol. 8988 89881A-1, 2014.
16. V. Mittal, L. G. Carpenter, J. C. Gates, J. S. Wilkinson and G. S. Murugan, "$GeTe_4$ channel waveguides for the mid-wave infrared spectral band", Photonics 2014, 12th International Conference on Fiber Optics and Photonics, T4B.4, OSA 2014.
17. J. Golden, H. Miller, D. Nawrocki and J. Ross, CS Mantech Technical Digest (2009).
18. L. G. Carpenter, H. L. Rogers, P. A. Cooper, C. Holmes, J. C. Gates and P. G. R. Smith, "Low optical-loss facet preparation for silica-on-silicon photonics using the ductile dicing regime", J.Phys. D: Appl. Phys. Vol. 46, 475103, 2013.
19. C. Vigreux-Bercovici, L. Labadie, J. E. Broquin, P. Kern and A. Pradel, "Selenide and telluride thick films for mid and thermal infrared applications", J. Optoelectron. Adv. M. 7, 2625 (2005).
20. V. Balan, C. Vigreux and A. Pradel, "Chalcogenide thin films deposited by radio-frequency Sputtering", J. Optoelectron. Adv. M. 6, 875 (2004).
21. C. Vigreux , E. Bonhomme, A. Pradel, "Te-rich Ge–As–Se–Te bulk glasses and films for future IR-integrated optics", J. Non. Cryst. Solids, Vol. 353, p. 1388–1391, 2007
22. X. H. Zhang, L. Calvez, V. Seznec, H. L. Ma, S. Danto, P. Houizot, C. Boussard-Pledel, J. Lucas, "Infrared transmitting glasses and glass-ceramics'', J. non-Crys. Solids, Vol. 352, p. 2411, 2006.
23. J. Nishii and T. Yamashita, "Infrared Fibre Optics", edited by J.S. Sanghera and I.D. Aggarwal, CRC Press, p.151, 1998
24. J. S. Yu, J. Y. Moon, S. M. Choi, and Y. T. Lee, "Fabrication of 1x8multimode-interference optical power splitter based on inp using ch4/h2 reactive ion etching," Japanese Journal of Applied Physics, Vol. 40, p. 634, 2001.